An International Journal of Optimization and Control: Theories & Applications
ISSN: 2146-0957 eISSN: 2146-5703
Vol.x, No.x, pp.xx-xx (2026)
https://doi.org/10.36922/IJOCTA026160064

RESEARCH ARTICLE

Model selection and performance evaluation of solar chimney systems using CFD and multivariate analysis with Chernoff faces

Alberto Hananel[1*], Rodolfo García[1], Alejandro Vera[1], Sandra Loaiza[1], and Iván Soto[2]

[1]Department of Engineering, Faculty of Engineering, Santo Toribio de Mogrovejo Catholic University, Chiclayo, Lambayeque, Peru
[2]Graduate School, Faculty of Engineering, Universidad Peruana Unión, Ñaña, Lima, Peru
ahananel@usat.edu.pe; rodolfo.garcia@usat.edu.pe; avlazaro@usat.edu.pe; sloayza@usat.edu.pe; ivansoto@upeu.edu.pe

ARTICLE INFO

Article history:
Received: April 18, 2025
Revised: June 1, 2025
Accepted: June 1, 2025
Published Online: June 24, 2025

Keywords:
Computational fluid dynamics (CFD)
Solar chimney power plants
Model selection
Nonlinear regression models
Chernoff faces
Multivariate analysis

AMS Classification 2010:
76M12; 76R10; 80A20; 76D05; 65N30

ABSTRACT

This paper presents an integrated study combining computational fluid dynamics (CFD) and multivariate statistical analysis for solar chimney optimization. The Manzanares plant was adopted as a reference model and simulated in ANSYS Fluent to generate a dataset for parametric evaluation. Eleven regression models were examined to describe air velocity as a function of the scale parameter, and their formulations were validated using statistical metrics and graphical multivariate analysis. The methodology introduces Chernoff faces as a visual–statistical tool to encode multiple performance indicators per model, enabling a structured comparison beyond conventional criteria. The power-law model proved the most suitable, showing strong goodness-of-fit, physical consistency, and stable behavior across scenarios. Specific equations were derived for different irradiance levels, and system efficiency and power output were estimated and compared with previous studies. The results confirm that geometric down-scaling significantly reduces performance. The proposed visual–statistical framework provides a robust and interpretable approach for model selection and performance assessment in solar energy systems, offering a novel and reproducible multivariate strategy for engineering design and optimization.

(cc) BY

1. Introduction

Statistics is a fundamental research tool for describing complex phenomena and developing structured problem-solving approaches based on data inference. In the context of higher education and scientific research, the increasing availability of large and heterogeneous datasets has made rigorous statistical methods indispensable for their processing, analysis and interpretation, as highlighted by Santos and Peña.[1] This necessity is particularly evident in multidisciplinary fields where physical, numerical and experimental variables must be jointly analysed.

Within this statistical framework, one of the most innovative contributions to the graphical representation of multivariate data was introduced by Chernoff.[2] His seminal work, The Use of Faces to Represent Points in k-Dimensional Space Graphically,proposed the use of parameterized human faces to encode high-dimensional information, exploiting the innate human ability to recognise patterns in facial structures. Each facial feature is associated with a quantitative variable, allowing complex relationships to be visually synthesised.

The relevance of this visual methodology was consolidated in subsequent decades as an exploratory alternative to traditional multivariate

*Corresponding Author

plots. Studies such as Flury and Riedwyl[3] emphasised the usefulness of graphical synthesis techniques for identifying latent structures in multidimensional datasets. More recently, Chernoff faces have also been applied by the authors in other analytical contexts, confirming their usefulness as a visual tool for multivariate interpretation and decision support as reported by Hananel *et al.*[4] However, as noted by Olmos,[5] the limited availability of specialised computational tools during the late twentieth century restricted the widespread application of advanced multivariate methods in experimental and engineering-oriented research.

In parallel, the field of renewable energy engineering experienced a major experimental milestone with the construction of the Manzanares solar chimney pilot plant in Spain, documented by Haaf *et al.*[6] This large-scale facility demonstrated the feasibility of electricity generation based on the greenhouse effect, where air heated under a collector reduces its density and rises through a central chimney, producing an airflow capable of driving turbines coupled to electrical generators. Although this experiment generated a substantial amount of physical and operational data, the application of advanced multivariate visual techniques such as Chernoff faces was not feasible at the time due to technological constraints. Recent experimental studies on heat transfer and energy performance in real systems have contributed to a deeper understanding of thermal processes, reinforcing the importance of combining physical measurements with numerical and statistical approaches, as shown by Jiménez *et al.*[7]

At present, these limitations have largely disappeared. The widespread availability of high-performance numerical solvers and statistical software has significantly expanded the analytical possibilities in both education and research, as highlighted by Cuicas Avila *et al.*[8] Nevertheless, several authors, including Medina Martínez,[9] point out that many statistical and mathematical advances remain underutilised in engineering applications. This is particularly evident in the analysis of complex systems where multiple physical variables interact nonlinearly. Even simple geometric considerations—such as classifying a solar chimney as cylindrical (convergent) or divergent based on inlet or outlet angles—suggest that design variables can be explored parametrically using multivariate visual tools. Under this perspective, structural features of a solar chimney can be directly associated with facial attributes in a Chernoff representation, enabling the identification of patterns that may not be evident through conventional univariate or bivariate analyses (see **Figure 1**).

Given that the main objective of this research is to perform a parametric evaluation of solar chimney design variables using the Chernoff Faces methodology, several indicators traditionally analysed independently in CFD-based regression models—such as air velocity, pressure, temperature and mass flow—are here examined simultaneously at a multivariate level. While numerical simulations allow the resolution of the systems of differential equations governing airflow and heat transfer within a solar chimney, the resulting expressions must be supported by a consistent mathematical interpretation in order to be considered valid approximations. In this sense, the proposed approach draws an analogy with multivariate statistics: just as facial features synthesise multiple dimensions of information, key physical variables in solar chimney design can be parameterised and visually integrated to guide performance optimisation and energy efficiency improvements.

Since the original Manzanares experiment, numerous studies have expanded the understanding of solar chimney systems and have used its results as a benchmark for validating advanced numerical simulations. For instance, Xu and Zhou[10] conducted CFD-based parametric analyses focusing on the relationship between the inlet and outlet areas of the chimney, demonstrating that appropriate geometric adjustments can significantly enhance energy efficiency. These findings were reinforced by Hu *et al.*,[11] who showed that non-cylindrical configurations can outperform classical designs in terms of mass flow and power output, revealing strong nonlinear dependencies on geometric ratios and collector dimensions.

Further contributions by Mebarki *et al.*[12] emphasised the impact of geometric scaling on energy generation, suggesting the feasibility of implementing solar chimney systems in urban environments. Complementarily, Murena *et al.*[13] established correlations between airflow velocity and environmental parameters, highlighting the dominant influence of solar irradiance and temperature. Collectively, these studies underline the need to combine theoretical formulations with CFD validation to improve system performance.

Recent literature has expanded SCPP analysis beyond steady irradiance assumptions through: (i) syntheses of technology limits, performance drivers, and future research needs;[14–17] (ii) crosswind-aware and wind-resilient configurations that quantify the sensitivity of mass flow

and pressure recovery to ambient wind conditions;[18–20] (iii) transient and storage-assisted operation addressing diurnal cycles and temperature fluctuations;[21,22] and (iv) turbine-focused modelling and design studies that highlight the influence of the power-conversion unit on predicted output.[23,24] These advances provide context for interpreting scale laws and for positioning multivariate model-selection tools—such as Chernoff faces—within modern CFD-supported design workflows.[25–29]

In the Peruvian context, only one significant experimental precedent has been identified by Velasco Lorenzo and Butler Blacker.[30] That work demonstrated the feasibility of a solar–wind chimney at a reduced scale but did not include a detailed parametric or mathematical analysis of performance variables.

This gap in the national and regional literature motivates the present research. By integrating CFD-derived physical variables with a multivariate visual framework based on Chernoff faces, this study improves the performance assessment of solar chimneys while enhancing the interpretability of complex numerical results. The proposed methodology introduces a cognitive dimension to engineering analysis, where optimisation decisions are supported by numerical evidence and visual recognition of multivariate patterns.

Finally, the optimisation of solar chimney design is framed as a long-term sustainable alternative in the context of climate change, particularly for regions such as Lambayeque, where climatic extremes affect vulnerable populations. In this sense, the present work contributes by combining mathematical modelling, statistical analysis and visual interpretation within a unified framework, reinforcing the role of interdisciplinary approaches in renewable energy research.

2. Materials and methods

The methodology was structured in two main stages. First, a partial replication of the classical CFD framework developed by Haaf for the Manzanares solar chimney pilot plant was carried out, using benchmark data reported in the literature to ensure consistency and physical validity of the numerical model. Second, a parametric design methodology aimed at enhancing solar chimney performance was developed, in which CFD-derived variables and analytical formulations were systematically analysed and validated through multivariate statistical techniques based on Chernoff Faces. The workflow integrated numerical simulation, mathematical modelling and statistical analysis, employing ANSYS Fluent for CFD computations, together with Statistica and R for regression modelling, variance analysis and graphical multivariate representation. The following sections describe the governing equations and physical assumptions, the simulation setup and boundary conditions, the classical performance formulations, and the statistical–visual framework adopted to evaluate and compare the resulting configurations.

2.1. Mathematical model

The behavior of fluid flow can be understood by tracking the displacement of fluid particles as a function of time. However, this approach is often tedious, so an efficient alternative is to study the velocity of the fluid, denoted as $\mathbf{V} = (v_x, v_y, v_z)$, where $\mathbf{V} = \left(\frac{\partial u}{\partial x}, \frac{\partial u}{\partial y}, \frac{\partial u}{\partial z}\right)$. The determination of these velocity components requires solving the differential equation of mass conservation in Cartesian coordinates, where ρ is the density:

$$\frac{\partial \rho}{\partial t} + \frac{\partial \rho v_x}{\partial x} + \frac{\partial \rho v_y}{\partial y} + \frac{\partial \rho v_z}{\partial z} = 0$$

This equation can be expressed more compactly as:

$$\frac{\partial \rho}{\partial t} + \operatorname{div}(\rho\, \mathbf{V}) = 0$$

Due to the geometry of the solar chimney, it is convenient to transform this equation to cylindrical coordinates (r, θ, z):

$$\frac{\partial \rho}{\partial t} + \frac{1}{r}\frac{\partial (\rho r v_r)}{\partial r} + \frac{1}{r}\frac{\partial (\rho v_\theta)}{\partial \theta} + \frac{\partial (\rho v_z)}{\partial z} = 0$$

where ρ is the fluid density and $\mathbf{v} = (v_r, v_\theta, v_z)$ is the velocity in the cylindrical system, with v_r, v_θ and v_z representing the radial, angular, and vertical components of velocity, respectively. In a solar chimney, it is generally assumed that $v_\theta = 0$. By rearranging the previous equation, the continuity equation is obtained:

$$\frac{\partial \rho}{\partial t} + \frac{\partial (\rho v_z)}{\partial z} + \frac{1}{r}\frac{\partial (\rho r v_r)}{\partial r} = 0$$

The momentum equation in the radial direction, with μ as the dynamic viscosity and p as the pressure, is:

$$\begin{aligned} \rho g - \frac{\partial p}{\partial r} + \mu\Big(&\frac{\partial}{\partial r}\left(\frac{1}{r}\frac{\partial (r v_r)}{\partial r}\right) \\ &+ \frac{\partial^2 v_r}{\partial z^2} - \frac{v_r}{r^2}\Big) \\ &= \rho\left(v_r\frac{\partial v_r}{\partial r} + v_z\frac{\partial v_r}{\partial z} + \frac{\partial v_r}{\partial t}\right). \end{aligned} \tag{1}$$

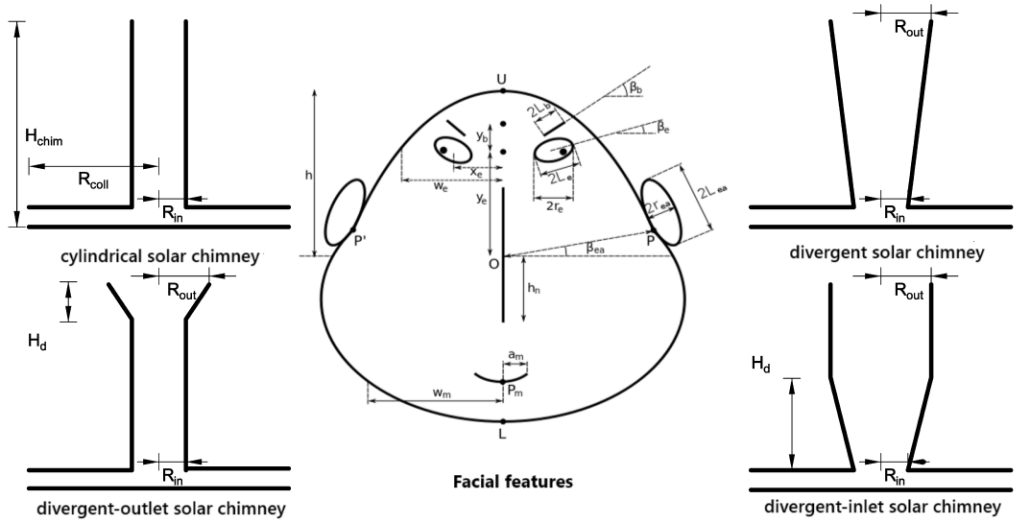


Figure 1. Conceptual mapping between solar-chimney geometric/operational parameters and Chernoff-face features for multivariate encoding. The diagram illustrates how collector/chimney geometry (e.g., radius, height, convergence/divergence patterns) can be associated with facial attributes to support visual comparison of configurations.

The momentum equation in the vertical direction is:

$$\rho g - \frac{\partial p}{\partial z} + \mu\left(\frac{1}{r}\frac{\partial}{\partial r}\left(r\frac{\partial v_z}{\partial r}\right) + \frac{\partial^2 v_z}{\partial z^2}\right) = \rho\left(v_r\frac{\partial v_z}{\partial r} + v_z\frac{\partial v_z}{\partial z} + \frac{\partial v_z}{\partial t}\right). \tag{2}$$

Replacing the components (v_r, v_z) for the calculation of temperature T and considering the radiative heat flux vector q_r in the energy equation, with λ as the thermal conductivity and C_p as the specific heat:

$$\frac{\partial(\rho C_p T)}{\partial t} + \frac{1}{r}\frac{\partial}{\partial r}\left(\rho r C_p v_r T\right) + \frac{\partial(\rho C_p v_z T)}{\partial z} = \frac{1}{r}\frac{\partial}{\partial r}\left(r\lambda\frac{\partial T}{\partial r}\right) + \frac{\partial}{\partial z}\left(\lambda\frac{\partial T}{\partial z}\right) - \mathrm{div}(q_r). \tag{3}$$

This equation, along with the continuity equation, can be reformulated in terms of temperature and pressure to compute the total energy per unit mass E:

$$\frac{\partial(\rho E)}{\partial t} + \nabla\cdot(\rho\mathbf{v}E + \mathbf{v}p) = \nabla\cdot(\lambda\nabla T) - \mathrm{div}(q_r)$$

where S represents source terms. In the case of a solar chimney, the parametric research focuses on the vertical component of velocity v_z.

2.2. Classical formulas for the efficiency and performance analysis of a solar chimney

The classic formulas for evaluating the efficiency and performance of a solar chimney are based on the definitions of pressure and volumetric flow rate. Pressure is determined by solving the system of partial differential equations presented in the momentum equation in Section 2.1. On the other hand, volumetric flow rate is calculated from the mass flow rate.

Mass flow, denoted by $\dot{m}$, represents the amount of mass transported through a cross-section of the system per unit time. This flow is related to the fluid density (ρ) and the volumetric flow rate (V). The volumetric flow rate is defined as the ratio of the mass flow to the fluid density: $V = \dot{m}/\rho$.

The power output, taking into account the pressure drop rate in the turbine (χ), is given by:

$$P = \eta_{turb}\chi\sqrt{1-\chi}\Delta p_{poten}V \tag{4}$$

where η_{turb} is the turbine efficiency, χ is the pressure drop rate across the turbine, $\Delta p_{\mathrm{poten}}$ is the potential pressure, and V is the volumetric flow rate.

If the parameter χ is not considered, the power is calculated with the formula:

$$P = \eta_{turb}\Delta p_{turb}V \tag{5}$$

where Δp_{turb} is the static pressure difference across the turbine, and the rest of the parameters are as previously described.

The values necessary for these calculations, extracted from the studies cited in Section 2.2, have been used as the basis for this analysis. These data, along with the methodology and results described by the mentioned authors, have been fundamental for evaluating the efficiency and performance of this research. The corresponding anal-

ysis is presented in Section 3.

2.3. Geometric parameters

The geometric parameters of the solar chimney, expressed in meters, are specified for the height and radius of both the chimney (H_{chim} and R_{chim}) and the collector ($H_{\text{collector}}$ and $r_{\text{collector}}$). These parameters were considered at full scale ($C = 1$) and are reported in **Table 1**. These values are essential for accurate modeling of the solar chimney. The adopted geometry is consistent with the previous work of Hananel *et al.*, where an aspect ratio of $AR = 6$ was used as a representative design condition.[31]

2.4. Modeling and meshing

A three-dimensional model of the Manzanares solar plant in Spain, as defined in Haaf *et al.*,[6] was implemented (**Figure 2A**). The cylindrical geometry with a disk-shaped collector was designed in SolidWorks and imported into ANSYS Fluent. A tetrahedral mesh was used (**Figure 2B**), together with the required boundary conditions and parameters, including density ($\rho = 1.103\,\text{kg/m}^3$) and ambient pressure (93.9 kPa).

Table 1. Some geometric parameters of the Manzanares solar chimney plant (adapted from Haaf *et al.*[6])

Scale (C)	H_{chim} (m)	R_{chim} (m)	$H_{\text{collector}}$ (m)	$r_{\text{collector}}$ (m)
Full scale (C=1, 1:1)	195	115	27	125

2.5. Boundary conditions

The following boundary conditions were set in Ansys Fluent:

- Wall:
  - Collector roof: Thermally insulated.
  - Chimney surface: Thermally insulated.
  - Transition section from collector to chimney: Thermally insulated.
  - Ground (effective heat flux = efficiency × irradiance): $0.294 \times 850 = 250\ \text{W/m}^2$.
- Inlet:
  - Collector inlet (no difference from ambient atmosphere).
  - Gauge pressure: 0 Pa.
  - Ambient ground-level temperature: 296.65 K (23.5 °C).
- Outlet:
  - Chimney outlet (no difference from ambient atmosphere).
  - Gauge pressure: 0 Pa.
  - Ambient ground-level temperature: 296.65 K (23.5 °C).
- Ventilation (Turbine):
  - Pressure drop (Δp_{turb}):
    - For simulated data: None (0 Pa).
    - For actual data (Validation): Non-zero (82.9 Pa).
  - Height at which it is located: 10 m.

2.6. Simulation parameters

After applying the boundary conditions and running the initial simulation, the Rayleigh number was calculated as

$$Ra = \frac{b}{a}\, g\, H_{\text{col}}^3 \frac{\Delta T}{v_z},$$

where v_z and ΔT were obtained from the simulation, and b and a denote the expansion coefficient and thermal diffusivity, respectively. The resulting Ra exceeded 1,000, indicating turbulent flow and motivating the reformulation of subsequent simulation conditions.

2.7. Physical-mathematical model underlying the simulation

The foundation of our methodology was based on the mathematical analysis of the parametric evaluation of the theoretical CFD variables. This analysis is structured in the following points, which constitute the pillars of the consistency of our framework:

(1) Parametric formula of the continuity equation: It is known that hydrostatic pressure is a physical formula that describes the behavior of fluids in equilibrium under gravity, linking pressure to the fluid density (ρ) and the height (H) in the form $P = \rho g H$. The velocity considered in the model (v_b or v_t) is the velocity in the radial direction (at the base or at the top of the chimney, respectively), i.e. the speed at which a point on the surface of the cylinder is moving toward or away from the central axis (positive if moving outward, negative if moving inward). It is also known from the continuity equation that the volumetric flow rate is constant at any cross-section of the duct; hence $A_1 v_1 = A_2 v_2$. Applying the continuity equation to the solar chimney gives $A_t v_t = A_b v_b$, which can be written in terms of the ratio of the top and

bottom surface areas of the chimney, allowing the parameter $\tau = \frac{A_t}{A_b}$ to be defined as:

$$\frac{v_b}{v_t} = \tau \tag{6}$$

(2) "Driving potential" ΔP: Known as the driving potential in a solar chimney, this potential is a "driving" force for airflow from the collector inlet to the top of the chimney. It essentially measures the pressure difference between the atmospheric pressure at ground level and the static pressure of the hot air stream at the base of the chimney (see Kröger and Blaine[32] and Ming *et al.*[33]):

$$\triangle P = P_0 - P_b. \tag{7}$$

Assuming constant air density and no pressure drop throughout the chimney, the static pressure at the base can be obtained using Bernoulli's equation:

$$P_b + \tfrac{1}{2}\rho v_b^2 + \rho g H_b = \text{const.} \tag{8}$$

At the base of the chimney, the elevation term vanishes ($H_b = 0$), so the Bernoulli constant reduces to $P_b + \frac{1}{2}\rho v_b^2$.

Similarly, at the top:

$$\text{const} = P_t + \tfrac{1}{2}\rho v_t^2 + \rho g H_t.$$

Equating constants:

$$P_b + \frac{1}{2}\rho v_b^2 = P_t + \frac{1}{2}\rho v_t^2 + \rho \cdot g \cdot H_t \tag{9}$$

Substituting $P_t = P_0 - \rho_0 g H_{\text{chim}}$ and rearranging yields:

$$\begin{aligned}\triangle P &= (\rho_0 - \rho) \cdot g \cdot H_{chim} \\ &+ \frac{1}{2}\rho(v_b^2 - v_t^2).\end{aligned} \tag{10}$$

Factoring v_b^2 in the difference, we obtain:

$$\begin{aligned}\Delta P &= (\rho_0 - \rho) g H_{\text{chim}} \\ &+ \tfrac{1}{2}\rho v_b^2 \left(1 - \left(\tfrac{v_t}{v_b}\right)^2\right).\end{aligned}$$

Using the continuity **Equation (6)**, this can be written in terms of height, base velocity, and the ratio τ:

$$\begin{aligned}\triangle P &= (\rho_0 - \rho) \cdot g \cdot H_{chim} \\ &+ \frac{1}{2}\rho(v_b^2)(1 - (\tau)^{-2})\end{aligned} \tag{11}$$

This indicates that ΔP increases with higher base velocity and higher τ (for $\tau > 1$), motivating the parametric investigation of τ. Since the Manzanares plant is cylindrical ($\tau = 1$), the second term vanishes, and classically:

$$\triangle P = (\rho_0 - \rho) \cdot g \cdot H_{chim} \tag{12}$$

(3) Parametric study of non-cylindrical chimneys: A solar chimney is called convergent (cylindrical) if it has zero inclination angle (top left in **Figure 1**), and divergent if it has a nonzero angle. The divergence is classified as fully divergent (top right), inlet divergent (bottom right), or outlet divergent (bottom left). When a chimney is divergent ($\tau > 1$), the dynamic pressure at the base has a greater impact, so the pressure difference heavily depends on the base velocity, regardless of the outlet. It is concluded that as τ increases, density and velocity are the variables that most influence the pressure variation, thereby increasing the chimney's efficiency. If the velocity is below 1 m/s, no increase in power is significant for Equation (11), regardless of τ; such an increase depends on the density ρ, which is small for air. Thus, for a solar chimney to be efficient, the bottom velocity must satisfy $v_b > 1$ m/s, and suitable locations should be selected. This justifies the focus on localities in the Lambayeque region, such as Olmos and Incahuasi. There average wind speeds are about 2.5 m/s and 4.8 m/s, respectively, with minimum values around 1.492 m/s. As discussed, these minimum values exceed 1 m/s, which enables the parametric study of solar chimneys. The data were obtained from NASA POWER Project.[34]

2.8. Selection of configurations and justification of the simulated design

The selection of the 30 solar chimney configurations used in this study is based on scientific precedents supporting the use of parametric analyses and CFD simulations to evaluate energy performance. Haaf's pioneering study on the Manzanares pilot plant is a key reference, as it explored geometric combinations under various environmental conditions through physical and numerical simulations. Subsequent investigations (e.g., Cuce and Murena) typically employing between 20 and 50 configurations. This range justifies the sample size used in the current study. Similarly, Xu showed that unconventional configurations can achieve notable performance, while Mebarki demonstrated through CFD that geometric simplification can preserve the model's explanatory power. These findings reinforce the relevance of considering multiple geometric scales within the experimental design.

Based on these precedents and considering computational efficiency and representativeness, a set

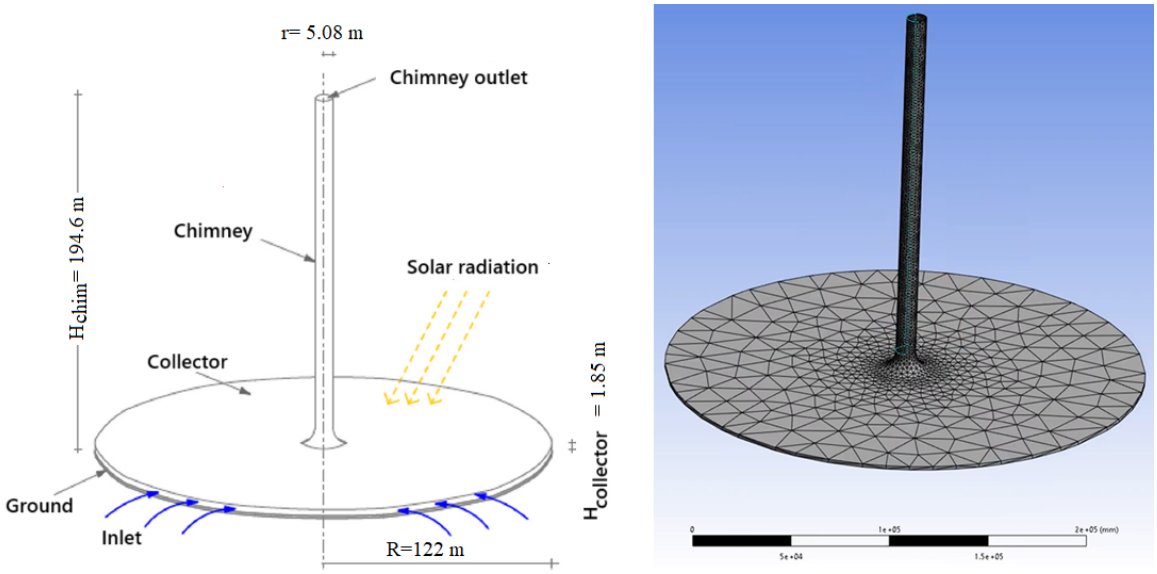


Figure 2. Modeling and meshing applied in the CFD analysis

of 30 simulations was defined, comprising 6 scaled geometries combined with 5 levels of solar irradiance. From a statistical perspective, this number of configurations is sufficient for estimating aggregated system parameters, since, under independence assumptions, the Central Limit Theorem allows approximating the distribution of the system's average performance by a normal distribution, even if the original responses are not normal. This provides a basis for comparative analysis and inference on the average behavior of the simulated solar chimneys.

2.9. CFD simulations in ANSYS Fluent

To capture small-scale effects independent of length and time scales, the κ-ε turbulence model was chosen, following common CFD practices by Maia and Silva,[20] Ferhati,[25] and Danook *et al.*[35] The model was implemented in ANSYS Fluent with appropriate solver and mesh configurations to ensure numerical robustness according to Ferhati *et al.*[25] The interaction between air velocity and pressure was analyzed using the finite volume method applied to the continuity, momentum, and energy equations.

For pressure estimation, a second-order Taylor expansion was adopted, leading to $\Delta p(v) \approx \Delta p(0) + \Delta p'(0)v + \frac{\Delta p''(0)}{2}v^2$, under the boundary conditions of Section 2.5, with $\Delta p(0) = 0$, $\Delta p'(0) = 0$, and $\Delta p''(0) = \rho$. This yields the simplified Bernoulli expression $\Delta p = \frac{1}{2}\rho v^2$, consistent with Murena *et al.*[13] The formulation was implemented in ANSYS Fluent using user-defined functions, with a convergence criterion of 10^{-6} and an inlet velocity of 1.3 m/s. **Table 2** summarizes the six scale factors considered in the CFD campaign and their corresponding geometric parameters. Simulations were then performed for each scale, generating the database used in the subsequent analyses. The results obtained (e.g., velocity, **Figure 3A**) are consistent with Mebarki *et al.*[12] The corresponding CFD results are shown in **Figure 3B**. Velocity contours from Mebarki *et al.*[12] (**Figure 4**) were used to extract extreme values at each scale. Although not explicitly reported in the source, the following values (e.g., 15.97, 11.60, 8.597, 63.03, 46.84, 39.62) were used for comparison with the database associated with the error analysis of velocity and turbulence parameters κ and ε (**Figure 5**).

2.10. Implementation of the CFD-based methodology using ANSYS Fluent

Data records obtained from selected physical variables in the simulations carried out in ANSYS Fluent were subsequently processed in the R environment. For this analysis, curvilinear estimation methods were used, with the parameter scale as the independent variable and velocity values obtained at different solar irradiance levels as the dependent variables.

A total of 11 regression models were evaluated: linear, quadratic, cubic, logarithmic, compound, growth, exponential, S-shaped, inverse, and power. Recent SCPP studies increasingly couple CFD with statistical surrogates and optimization frameworks (e.g., RSM/DOE or ML-based predictors) to accelerate design-space exploration and reduce the cost of parametric campaigns. This trend motivates the present regression-based workflow, as seen in Cuce *et al.*[26]

and Sundararaj *et al.*[36] For each model, the constants associated with the regression equations were estimated, as well as their graphical representation, allowing visual and statistical comparison of simulated data. In addition, the main statistical indicators for each model were calculated, including the coefficient of determination (R^2), the standard error of the estimate, and the ANOVA test, to evaluate the overall significance of the fitted model. This analysis enabled selecting the models with the best explanatory capability based on the behavior observed in the numerical simulations.

Table 2. Scale factors used in the CFD campaign and corresponding geometric parameters (scaled from the Manzanares full-scale reference)

Scale C	H_{chim} (m)	R_{chim} (m)	$H_{\text{collector}}$ (m)	$r_{\text{collector}}$ (m)
1.00000	195.00	115.00	27.00	125.00
0.50000	97.50	57.50	13.50	62.50
0.25000	48.75	28.75	6.75	31.25
0.12500	24.38	14.38	3.38	15.63
0.06250	12.19	7.19	1.69	7.81
0.03125	6.09	3.59	0.84	3.91

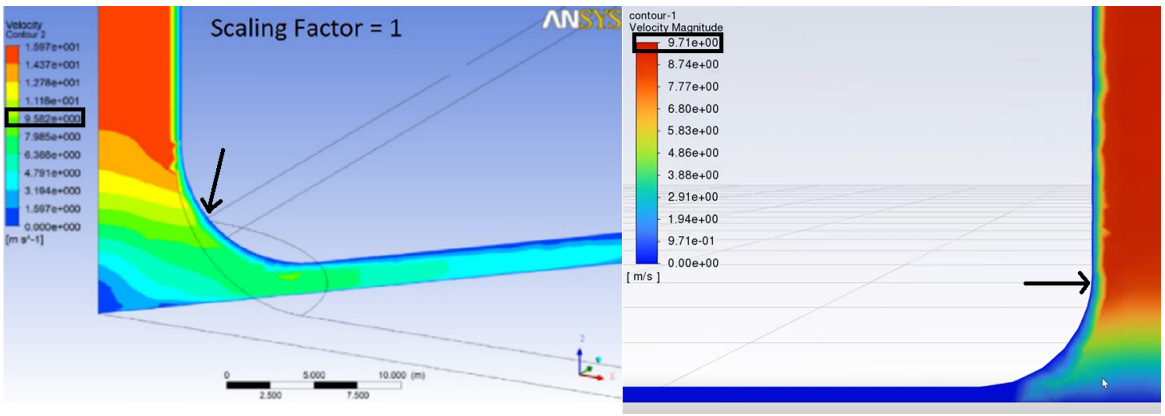


Figure 3. Results obtained from the replicated simulation of the Manzanares experiment for velocity with a scale factor of $C = 1$ and an irradiance of $W = 1000$ W/m^2

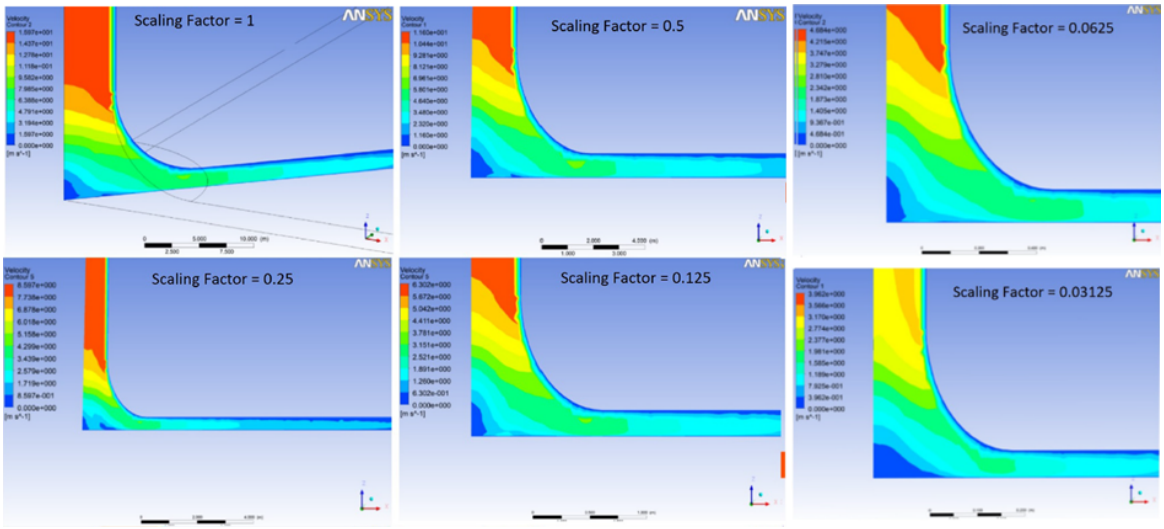


Figure 4. Illustrative velocity simulation results by Mebarki at six different scales, used to extract extreme values for comparison

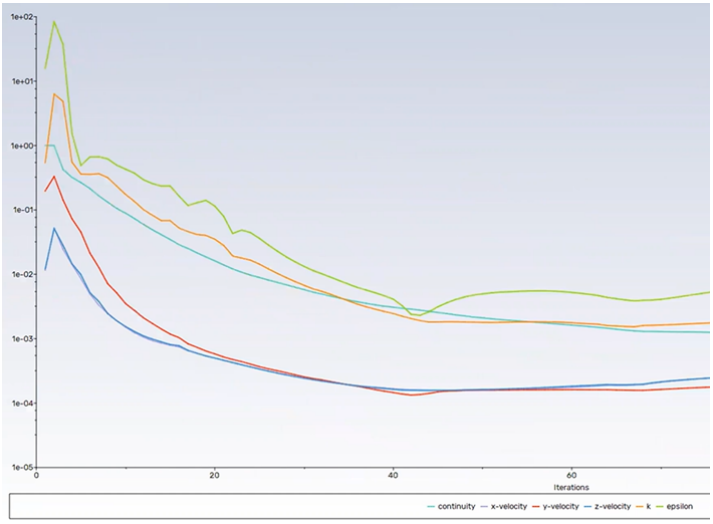


Figure 5. Error plot for the velocity variable and turbulence parameters κ and ε, derived from the replicated CFD simulation of the Manzanares experiment at $C = 1$ and $W = 1000$ W/m^2

2.11. Parametric evaluation using Chernoff Faces

In this study, the Chernoff Faces methodology was implemented as a graphical tool to represent multivariate interactions in solar chimney design. This technique assigns numerical values of variables to facial features of a schematic face, facilitating the visual interpretation of complex configurations. Fifteen facial features were considered, each linked to a different variable, following the coding "RFi" (Facial Feature i). The features used were: face width (RF1), ear height (RF2), upper-face height (RF3), upper-face width (RF4), lower-face width (RF5), nose length (RF6), vertical position of the mouth (RF7), mouth curvature (RF8), mouth length (RF9), eye height (RF10), distance between the eyes (RF11), eye tilt (RF12), pupil eccentricity (RF13), eye diameter (RF14), and pupil position (RF15).

2.12. Association of statistical variables to facial features

Fifteen statistical variables were considered, grouped into three categories: summary variables, ANOVA-derived variables, and variables associated with regression model coefficients. These variables were assigned to the fifteen facial features (RF1–RF15) defined earlier, following a direct correspondence $RFi \leftrightarrow Vi$. This correspondence enabled generating graphical representations capable of synthesizing the observed multivariate patterns, as illustrated in **Figure 6**, thus facilitating both model comparison and the identification of optimal solar chimney design profiles. The summary variables included the coefficient of determination R^2 (V1) and the standard error of the estimate (V2). The variables related to the analysis of variance were: the sum of squares of regression (V3), the sum of squares of the residual (V4), the degrees of freedom of the regression (V5), the mean square of regression (V6), the F statistic (V7) and its significance level (V8). Finally, among the variables related to the model coefficients were considered: the model constant (V9), the first coefficient of the model (V10), the standardized Beta coefficient (V11), the t-statistic for the constant (V12) and for the variable (V13), and their corresponding significance levels (V14, V15). This systematic assignment allows us to generate Chernoff faces where each facial attribute encoded a different statistical aspect of the regression models, enabling intuitive visual comparison.

3. Results

3.1. Regression results obtained in R

The statistical results derived from the numerical simulations performed in ANSYS Fluent were processed in the R environment, applying curvilinear fitting with a tolerance of 0.0001. Eleven regression models were evaluated, with the axial velocity (v_z), denoted here as V_m, as the dependent variable, and the system's geometric scale as the independent variable. For each model, adjusted equations were generated and relevant values from three statistical blocks were extracted: the model summary, the ANOVA table, and the model coefficients. Four models (inverse, quadratic, cubic, and power) were selected as representative models to be compared using Chernoff face visualizations, the results of which are detailed in **Table 3**, panels (a)–(d).

Table 3. Statistical results of the fitted regression models obtained in R

(a) Inverse regression model

Model Summary				
R	R^2	**Adjusted** R^2	**Std. Error of Estimate**	
0.794	0.630	0.538	2.331	
ANOVA				
Source	**Sum of Squares**	**df**	**Mean Square**	**F / Sig.**
Regression	37.039	1	37.039	6.819 / 0.059
Residual	21.728	4	5.432	–
Total	58.767	5	–	–
Coefficients				
Variable	**Coefficient (B)**	**Std. Error**	**Beta**	**t / Sig.**
1/scale	−0.229	0.088	−0.794	−2.611 / 0.059
Constant	8.235	1.325	–	6.214 / 0.003

(b) Quadratic regression model

Model Summary				
R	R^2	**Adjusted** R^2	**Std. Error of Estimate**	
0.997	0.995	0.991	0.320	
ANOVA				
Source	**Sum of Squares**	**df**	**Mean Square**	**F / Sig.**
Regression	58.459	2	29.230	284.912 / 0.000
Residual	0.308	3	0.103	–
Total	58.767	5	–	–
Coefficients				
Variable	**Coefficient (B)**	**Std. Error**	**Beta**	**t / Sig.**
x^2	−7.081	1.492	−0.811	−4.748 / 0.018
x	16.312	1.580	1.764	10.326 / 0.002
Constant	2.047	0.250	–	8.190 / 0.004

(c) Cubic regression model

Model Summary				
R	R^2	**Adjusted** R^2	**Std. Error of Estimate**	
1.000	0.999	0.998	0.135	
ANOVA				
Source	**Sum of Squares**	**df**	**Mean Square**	**F / Sig.**
Regression	58.730	3	19.577	1072.970 / 0.001
Residual	0.036	2	0.018	–
Total	58.767	5	–	–
Coefficients				
Variable	**Coefficient (B)**	**Std. Error**	**Beta**	**t / Sig.**
x^3	14.886	3.860	1.735	3.856 / 0.061
x^2	−29.069	5.737	−3.329	−5.067 / 0.037
x	23.903	2.078	2.584	11.501 / 0.007
Constant	1.606	0.156	–	10.320 / 0.009

(d) Power regression model

Model Summary				
R	R^2	**Adjusted** R^2	**Std. Error of Estimate**	
1.000	1.000	1.000	0.000	
ANOVA				
Source	**Sum of Squares**	**df**	**Mean Square**	**F / Sig.**
Regression	1.858	1	1.858	1.003×10^{11} / < 0.001
Residual	0.000	4	0.000	–
Total	1.858	5	–	–
Coefficients				
Variable	**Coefficient (B)**	**Std. Error**	**Beta**	**t / Sig.**
ln(scale)	0.470	0.000	1.000	316760.990 / < 0.001
Constant	11.324	0.000	–	321078.645 / < 0.001

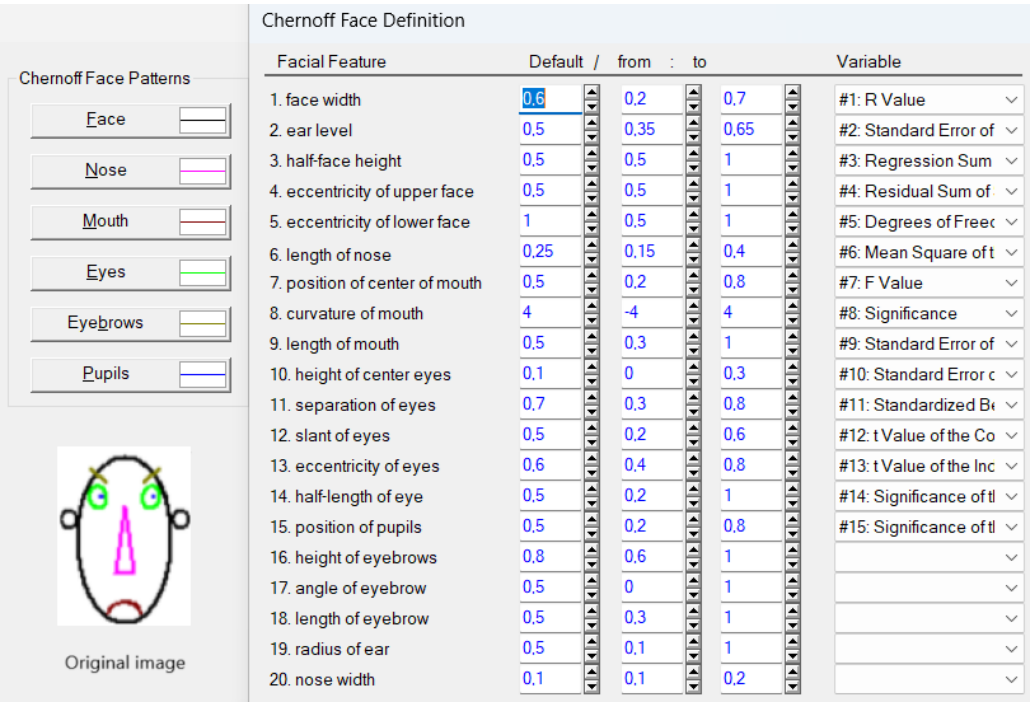


Figure 6. Facial attributes of Chernoff Faces mapped with statistical analysis variables for regression model selection in the parametric study of solar chimneys

Finally, the data from the 11 models were summarized in a table structured with 15 statistical variables per model (**Tables 4** and **5**). These tables served as the basis for constructing the faces in the multivariate visual analysis. Although consistent results were obtained for other simulated variables such as pressure, mass flow, and temperature, only those corresponding to V_m are reported, as it is the most relevant variable according to the literature review.

3.2. Model selection using Chernoff Faces

A visual analysis using Chernoff Faces was applied to identify the most suitable nonlinear regression model among eleven candidates: linear (C1), logarithmic (C2), inverse (C3), quadratic (C4), cubic (C5), compound (C6), power (C7), S-curve (C8), growth (C9), exponential (C10), and logistic (C11). The selection was based on the highest correlation coefficient values (R) and the generated facial representation, which allowed us to discard eight models and focus the evaluation on the three most promising ones.

3.3. Validation and permutation of variables

To address potential biases in the visual representation, permutations were performed in the assignment of variables to facial features, analyzing three scenarios: default configuration (**Figure 7**), features expressing overconfidence (**Figure 8**), and features reflecting emotional stability (**Figure 9**). The final selection was based on the intersection of the "best faces" across the three contexts.

The criteria considered included error deviation, sum of squares (regression and residual), degrees of freedom, mean square, F-value and its significance, as well as standard errors and t-values for both the constant and the independent variable. Additionally, standardized Beta coefficient and associated significance levels were considered. Based on this cross-evaluation, it was concluded that the most robust and consistent regression model was the power model, represented in **Figure 10**, as it displayed the most favorable facial features across the three visual scenarios considered.

3.4. Statistical confirmation of the selected model

Table 6 presents the coefficients estimated in R for the power regression model, which achieved a perfect fit on the simulated data. The final equation for air velocity (V_m), as a function of the geometric scale (C), was defined as:

$$V_m = 14.177 \cdot C^{0.416} \quad (\mathrm{m/s})$$

This expression matches very closely the one proposed by Mebarki *et al.*, who obtained for an irradiance of 1000 W/m^2 the equation $V_m = 14.17 \cdot C^{0.415}$, reinforcing the validity and replicability of the present model.

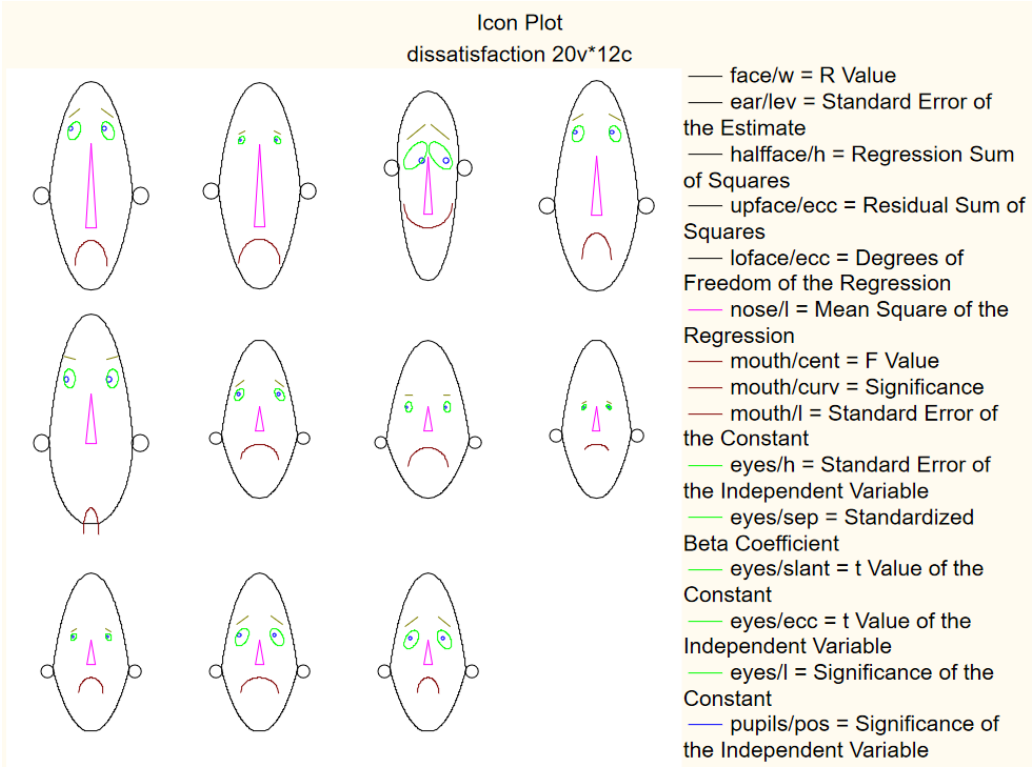


Figure 7. Chernoff faces for 11 candidate regression models (Scenario 1). Each face encodes 15 statistical indicators, enabling structured multivariate comparison.

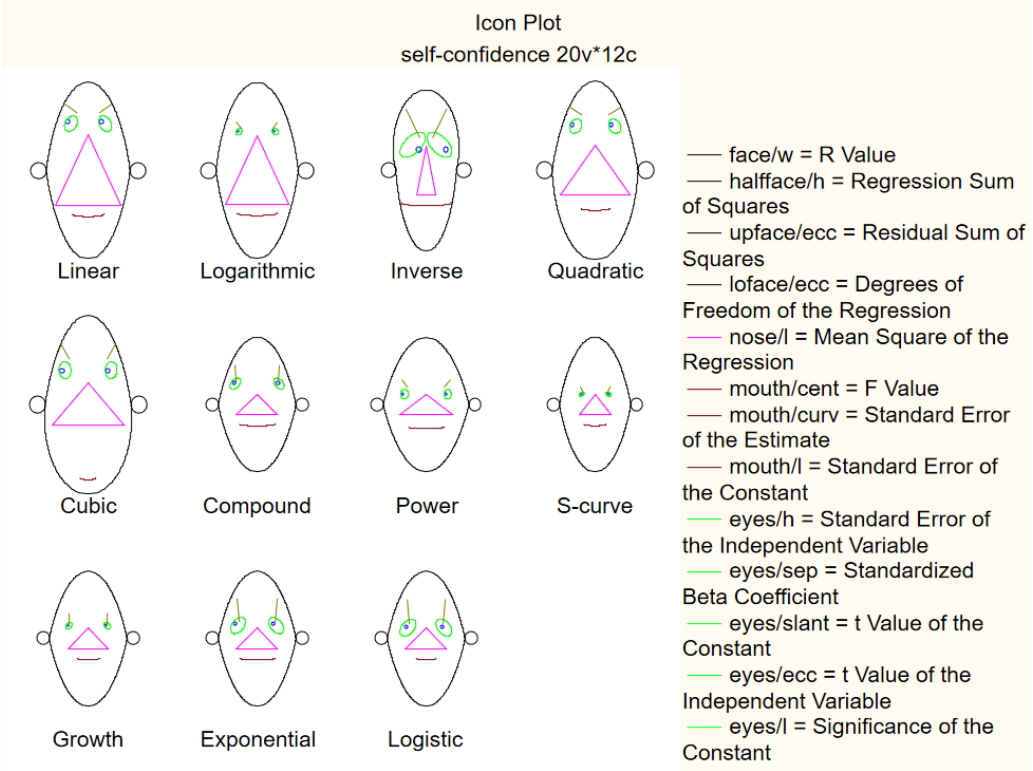


Figure 8. Chernoff faces for the 11 candidate regression models (Scenario 2). Each face encodes 15 statistical indicators (fit, ANOVA, and coefficient tests) mapped to facial features, enabling structured multivariate comparison across models, with a configuration reflecting self-confidence.

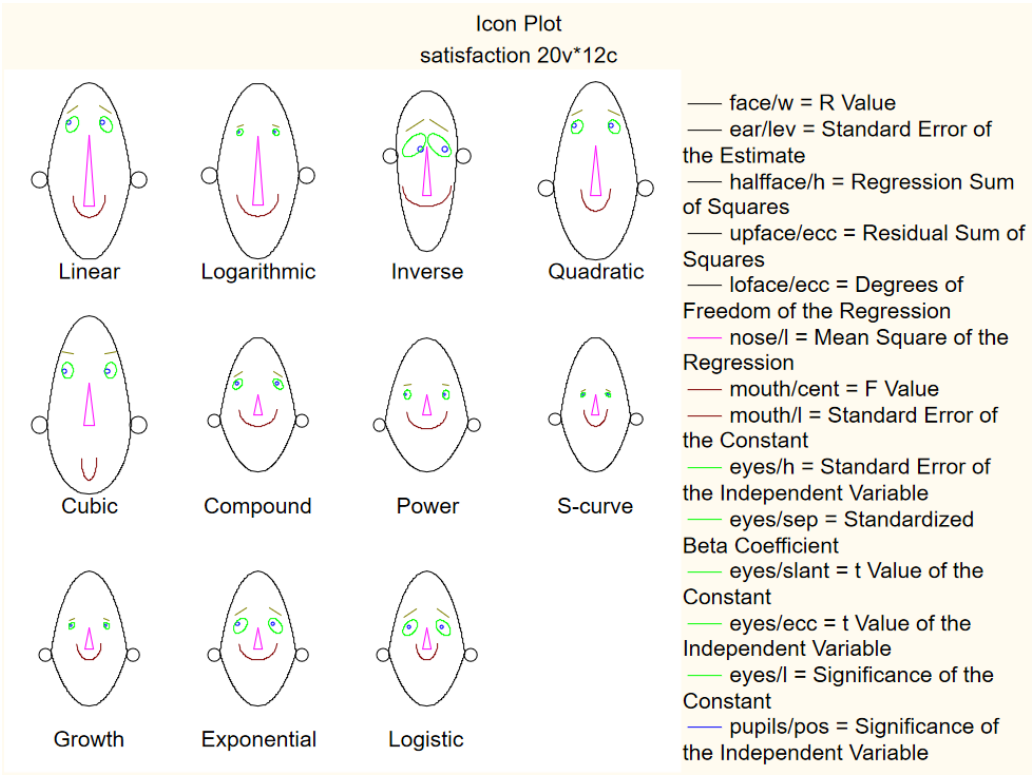


Figure 9. Chernoff faces for the 11 candidate regression models (Scenario 3). Each face encodes 15 statistical indicators (fit, ANOVA, and coefficient tests) mapped to facial features, enabling structured multivariate comparison across models, with a configuration reflecting satisfaction.

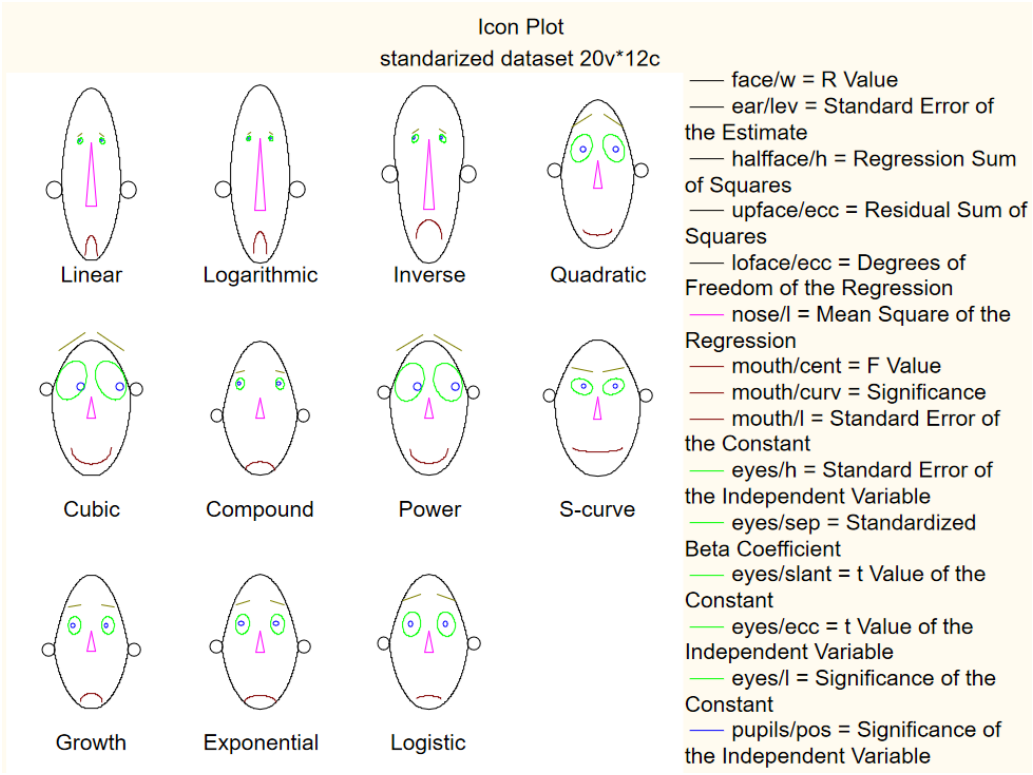


Figure 10. Chernoff Faces confirmatory analysis using a standardized dataset. The mapping of statistical indicators to facial features allows consistent visual interpretation of model performance, supporting the robustness of the power model relative to alternative regression forms.

Table 4. Dataset of 11 regression models with selected statistical measures for velocity V_m (fit and ANOVA metrics)

Model	R	Std. Error	Reg SS	Res SS	Reg df	Reg MS	F	Sig
Linear	0.981	0.985	101.522	3.883	1.000	101.522	104.590	0.001
Logarithmic	0.967	1.303	98.611	6.793	1.000	98.611	58.063	0.002
Quadratic	0.997	0.320	98.311	0.456	2.000	49.155	477.632	< 0.001
Cubic	1.000	0.135	58.230	0.036	3.000	19.410	1070.00	0.001
Exponential	0.975	0.070	98.217	26.495	1.000	98.217	75.574	0.001
Power	1.000	0.000	1.858	0.000	1.000	1.858	1.003×10^{11}	< 0.001
Inverse	0.794	2.331	37.039	21.728	1.000	37.039	6.819	0.059
Logistic	0.987	0.551	69.331	4.542	2.000	34.666	54.394	< 0.001
S-Curve	0.991	0.407	58.366	1.853	2.000	29.183	180.31	< 0.001
Growth	0.959	0.942	86.466	11.529	1.000	86.466	91.792	0.000
Compound	0.966	0.802	82.105	5.034	1.000	82.105	102.323	< 0.001

Table 5. Dataset of 11 regression models with selected statistical measures for velocity V_m (coefficients and tests)

Model	Std. Error (Const)	Std. Error (Var)	Beta	t (Const)	t (Var)	Sig (Const)	Sig (Var)
Linear	0.560	1.189	0.981	8.086	10.227	0.001	0.001
Logarithmic	0.943	0.449	0.967	15.324	7.620	0.002	0.002
Quadratic	0.163	0.333	0.997	20.011	13.169	< 0.001	0.001
Cubic	0.156	0.271	0.998	10.320	11.501	0.009	0.007
Exponential	0.726	0.296	0.975	12.107	8.392	0.001	0.004
Power	0.000	0.000	1.000	316760.99	321078.65	< 0.001	< 0.001
Inverse	0.088	1.325	0.794	-2.611	6.214	0.059	0.003
Logistic	0.268	0.874	0.987	14.849	7.968	< 0.001	0.012
S-Curve	0.365	0.392	0.991	10.094	7.441	0.001	0.012
Growth	0.782	2.212	0.959	11.787	8.805	0.002	0.008
Compound	0.593	1.201	0.966	11.256	9.229	0.002	0.000

Table 6. Estimated coefficients in R for the power regression model

Variable	B	SE	Beta	t	Sig.
Constant	14.177	0.000	1.000	2.737×10^5	< 0.001
$\ln(C)$	0.416	0.000	1.000	2.388×10^5	< 0.001

3.5. Independence from chosen scenarios in model selection

To confirm that the choice of model was not solely dependent on the proposed visual scenarios, the database was standardized and a new analysis using Chernoff Faces was performed. This new scenario focused on faces representative of "statistical normality", as shown in **Figure 11**. In this context, the most favorable models were the fifth (cubic) and the seventh (power), although the fourth (quadratic) could also be considered acceptable. Given the visual similarity between the faces corresponding to models 5 and 7, both were individually analyzed without standardization. Considering that the most influential variables in a regression model are usually statistical significance and the R value, a permutation was performed excluding both variables to observe the impact of the remaining parameters. This strategy is supported by Chrobak *et al.*,[37] who suggests that "when only a few variables are considered, particular attention must be paid to which facial features are changing". In **Figure 12**, it is evident that even without considering these two key variables, model (power) continues to present the most balanced face, confirming its robustness as the selected model.

3.6. Validation of selected model by Chernoff faces

A normality test was applied to the differences between the predictions of the cubic and power

models. As summarized in **Table 7**, the Shapiro–Wilk normality test yielded a value of $W = 0.851$ with $p = 0.162$, indicating that the differences follow a normal distribution. The paired sample Pearson correlation was extremely high ($r = 0.999$, $p < 0.001$), indicating an almost perfect correspondence in the prediction patterns without implying exact collinearity. A paired samples t-test yielded $t = -1.147$ (reported as $|t| = 1.147$) with $p = 0.303$, indicating that there are no statistically significant differences between the means of the two models. Together, these results support the statement that both models are statistically equivalent in predictive capacity. However, the power model was chosen for its greater functional simplicity, theoretical coherence with the physical behavior of the phenomenon, and more balanced visual representation according to the Chernoff faces methodology.

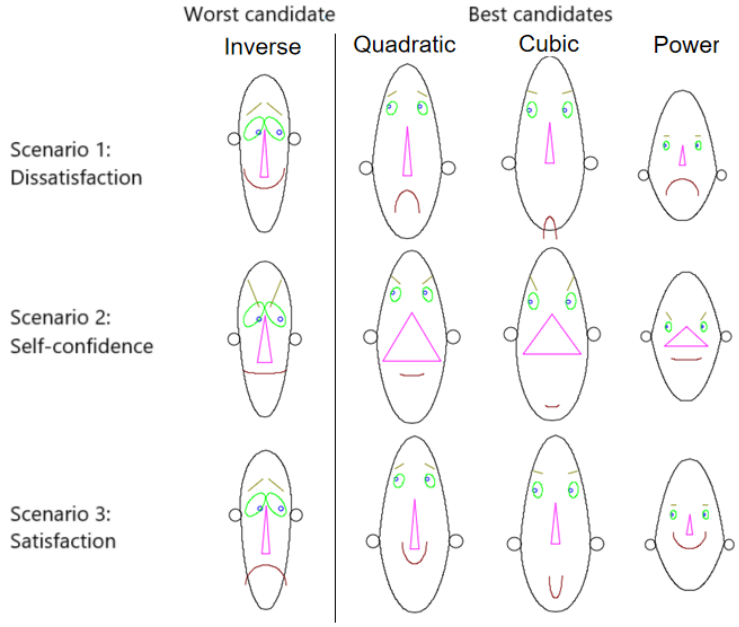


Figure 11. Chernoff Faces representation of the 11 candidate regression models across three scenarios. Each face encodes 15 statistical indicators related to goodness-of-fit, ANOVA, and coefficient significance, enabling a structured multivariate comparison. The power model consistently emerges as the strongest candidate across all scenarios.

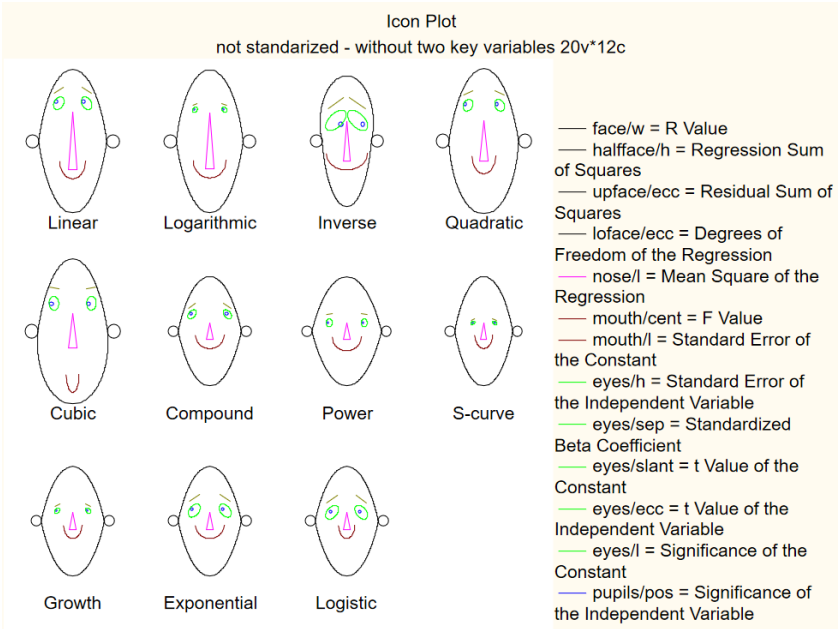


Figure 12. Chernoff Faces: second confirmatory analysis without standardization or key variables

Table 7. Statistical comparison of cubic and power models at 1000 W/m^2

Test	**Statistic**	***p*-value**
Shapiro–Wilk test	0.851	0.162
Paired Pearson r	0.9999	< 0.001
Paired Student's t	1.147	0.303

3.7. Theoretico-experimental validation

The validity of the obtained power regression model is reinforced by comparison with the equation reported by Mebarki *et al.*,[12] who, using experimental data from the Manzanares solar plant, proposed a similarly structured model for air velocity. However, that study does not detail the methodological or statistical criteria supporting model selection. In contrast, the present study incorporates a combined theoretical–statistical approach that rigorously justifies the selection of the most appropriate regression model.

3.8. CFD equations with statistical justification

Based on the statistical analysis of simulated data under different irradiance conditions, the power regression equation best represents the behavior of air velocity (V_m) as a function of the scale parameter (C) in a solar chimney. The expressions obtained for five irradiance levels (W) are given below:

$$\begin{cases} V_m = 14.17 \cdot C^{0.415}, & W = 1000\ \text{W/m}^2 \\ V_m = 13.45 \cdot C^{0.417}, & W = 800\ \text{W/m}^2 \\ V_m = 12.87 \cdot C^{0.429}, & W = 600\ \text{W/m}^2 \\ V_m = 12.24 \cdot C^{0.448}, & W = 400\ \text{W/m}^2 \\ V_m = 11.32 \cdot C^{0.470}, & W = 200\ \text{W/m}^2 \end{cases} \tag{13}$$

These expressions are not only consistent with the physical principles governing fluid dynamics in solar chimneys, but have also been validated through both statistical and visual contrast using Chernoff Faces.

3.9. Graphical comparison of models

To reinforce the previous findings, a graphical comparison of the velocity curves obtained from the power regression for different irradiance levels is presented. As shown in **Figure 13A**, the results generated using R accurately replicate the characteristics reported in the literature. In contrast, **Figure 13B** presents the original results obtained by Mebarki *et al.*[12]

3.10. Efficiency and performance results

Based on the velocity values obtained in the previous section, the power output of the system was calculated using the mathematical models developed in Section 2.2. Noted that predicted power can be sensitive to the representation of the turbine (power conversion unit); recent turbine-oriented numerical studies by Salim *et al.*[23] and Caicedo and Johansen[24] for SCPPs highlight that turbine modelling choices can alter the inferred pressure drop and output estimates. Using experimental data from Xu and Zhou,[10] a mass flow of $\dot{m} = 987.50$ kg/s (according to MFR in **Table 5**) and an air density of $\rho = 1.103$ kg/m^3 (according to **Table 3**) were considered, which allows us to calculate the volumetric flow as:

$$V = \frac{\dot{m}}{\rho} = \frac{987.50\ \text{kg/s}}{1.103\ \text{kg/m}^3} \approx 895.29\ \text{m}^3/\text{s} \tag{14}$$

For the calculation of power output under different conditions, the following configurations were used:

- With the geometric efficiency parameter χ (**Eqation 4**): The turbine efficiency was taken as $\eta_{\text{turb}} = 0.83$ (see Haaf *et al.*,[6] **Table 3** in Cuce *et al.*,[38] and Xu and Zhou[10]), $\chi = 2/3$, $\Delta p_{\text{poten}} = 68.32$ Pa, and the value of V obtained above.

  The resulting calculation is given by

  $$P = 0.83\,(2/3)\,\sqrt{1-(2/3)}\,(68.32)(895.29),$$

  which yields $P \approx 19.5$ kW. This value is consistent with that reported in **Table 5** of Xu and Zhou,[10] supporting the validity of the proposed formulation.
- Without the parameter χ (**Eqation 5**): $\Delta p_{\text{turb}} = 82.9$ Pa (**Table 3** in Xu and Zhou[10]) was used and $V = 574.07$ m^3/s was obtained. The power was obtained as:

  $$P = 0.83 \cdot 82.9 \cdot 574.07 \approx 39.5\ \text{kW}.$$

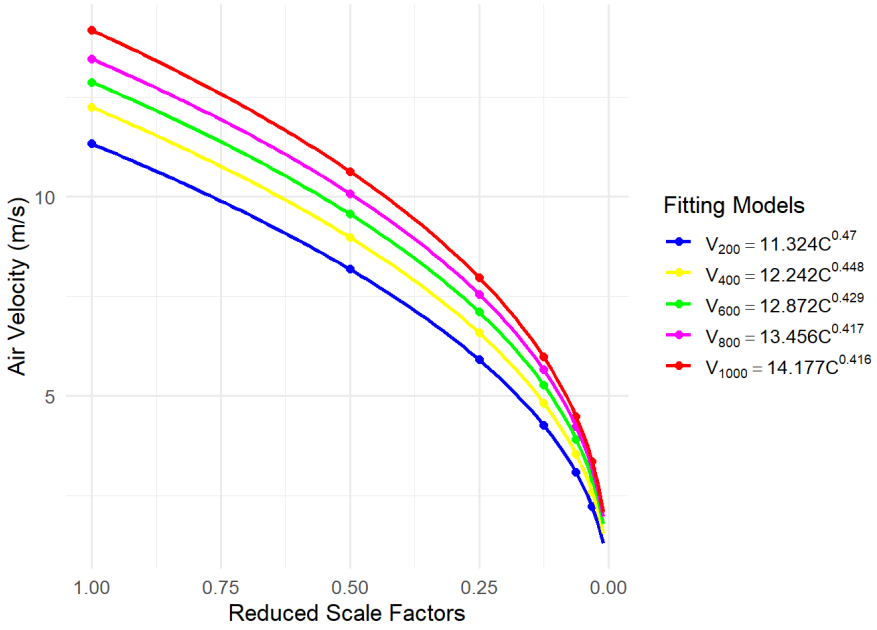
  This result approximates the ideal experimental power (40 kW) and the experimentally reported value at the Manzanares plant (36 kW) according to Haaf *et al.*,[6] demonstrating the effect of the parameter χ on overall system efficiency.

4. Discussion

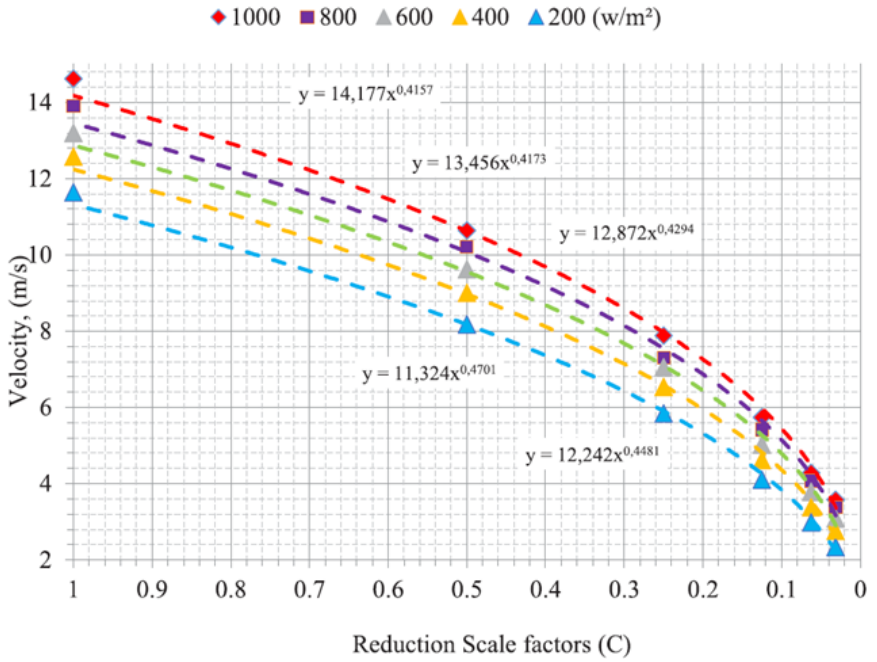
4.1. Comparison with previous results

Results from the paper of Xu and Zhou:[10]

Velocity, pressure difference, mass flow, efficiency, and electric power decrease as the scale factor (C) is reduced. In addition, empirical equations were proposed to describe the variation of air velocity, pressure, temperature, mass flow, and electric power as functions of reduced scale factors relative to a reference solar plant.



(A)



(B)

Figure 13. Comparison of replicated and reference CFD results for air velocity (V_m) as a function of scale factor (C) under different irradiance levels. (A) Results obtained using the proposed power regression model. (B) Reference CFD results adapted from Mebarki *et al.*[12]

Results of the present study: The present results confirm that system performance systematically decreases with scale reduction, in agreement with previous findings. In contrast to prior studies, a statistically grounded framework is introduced to justify the selection of regression models—particularly the power-law formulation—for

modeling key variables as functions of the scale parameter.

4.2. Interpretation of findings

The present work extends the classical CFD-based approach by incorporating multivariate statistical analysis and visual representation through Chernoff faces. Three visual configurations and multiple statistical scenarios were analyzed to assess the robustness of the selected model. The power regression model was consistently identified as the most suitable due to its numerical performance, visual coherence, structural simplicity, and theoretical consistency with the literature. Additionally, key geometric variables not extensively addressed in previous studies — such as chimney height, radius, and collector dimensions —were explicitly integrated, allowing a clearer interpretation of how geometric scaling affects overall system performance.

4.3. Added value of the visual–statistical approach

The use of Chernoff faces enabled the simultaneous representation of 15 performance and design variables within a single schematic structure. This approach facilitated the comparison of regression models and revealed complex multivariate patterns that may remain hidden in purely numerical analyses.

The inclusion of permutation schemes and variable standardization demonstrated that the methodology is robust under different configurations and supports model selection without introducing visual bias. Furthermore, the graphical patterns consistently reflected the degradation of system performance with scale reduction, reinforcing the quantitative findings and supporting the integration of visual tools with inferential statistics.

4.4. Implications and future work

The results provide a robust modeling framework for evaluating solar chimney performance under varying scales and irradiance levels, while introducing a replicable methodology for visualization-assisted design. This approach supports prototype optimization, evaluation of alternative configurations, and reduction of modeling uncertainty in early design stages.

However, real-world performance may deviate from the steady-state conditions considered in this study. Environmental factors such as ambient crosswinds, transient irradiance, and temperature fluctuations affect buoyancy-driven flow and system efficiency. Recent studies address these effects through wind-resistant configurations, transient modelling with thermal energy storage, and site-specific analyses quantifying the impact of local meteorology on system performance and techno-economic indicators,[17–19] according to Arefian *et al.*,[21] Nie *et al.*,[28] and Abo-Zahhad *et al.*[39]

From a practical perspective, the proposed workflow serves as a decision-support layer on top of CFD simulations: (i) to identify compact and stable functional relationships under varying conditions, and (ii) to guide parametric optimization — including multi-objective and AI-assisted approaches—towards configurations that balance performance, cost, and robustness. Future research should extend this framework to unsteady CFD scenarios (e.g., diurnal cycles), stochastic wind conditions, and multi-site datasets, and integrate it with advanced optimization and control strategies, as demonstrated by Cuce *et al.*,[26] Mandal *et al.*,[27] Salameh *et al.*,[29] and Torkfar *et al.*[40]

5. Conclusion

This study presents a CFD-based parametric analysis of solar chimney systems combined with a multivariate statistical framework for model selection. The main findings can be summarized as follows:

First, the replication of the Manzanares configuration provided a consistent dataset for evaluating the relationship between air velocity and the scale parameter. Among eleven regression models, the power-law formulation demonstrated the best performance, combining statistical robustness, physical interpretability, and stability across scenarios.

Second, the integration of Chernoff faces enabled a novel multivariate evaluation strategy, allowing the simultaneous interpretation of multiple statistical indicators. This approach extends traditional model selection methods by incorporating visual–statistical coherence as a complementary decision criterion.

Third, the results confirm that geometric downscaling significantly reduces system performance, highlighting the importance of scale effects in the design and feasibility of solar chimney power plants. The derived power-law expressions across different irradiance levels provide compact and transferable tools for preliminary design and rapid estimation.

From a methodological perspective, the proposed CFD–statistical–visual framework constitutes a relevant contribution, offering a structured

and reproducible approach for model selection and performance assessment in multivariate engineering problems.

Finally, a limitation of this study lies in the use of steady-state simulations under controlled boundary conditions. Future work should incorporate transient effects, ambient wind variability, and site-specific conditions, as well as extend the framework toward multi-objective optimization and control-oriented design.

Acknowledgments

The authors acknowledge the Plataforma Solar de Almería (PSA–CIEMAT), Spain, for the technical visit and thank Dr. María José Jiménez Taboada for her support and insights into solar chimney system.

Funding

This research was financially supported by the Santo Toribio de Mogrovejo Catholic University (USAT), Peru (005-2025-USAT-RTDO).

Conflict of interest

The authors declare they have no competing interests.

Author contributions

Conceptualization: Alberto Hananel
Data curation: Sandra Loaiza
Formal analysis: Alberto Hananel
Investigation: Alberto Hananel, Rodolfo García
Methodology: Alberto Hananel
Project administration: Alberto Hananel
Software: Alberto Hananel
Supervision: Iván Soto
Validation: Alberto Hananel
Visualization: Alberto Hananel
Writing–original draft: Alejandro Vera
Writing–review & editing: Alberto Hananel

Availability of data

The datasets generated and analyzed during the current study are available from the corresponding author on reasonable request.

AI tools statement

The authors confirm that no artificial intelligence (AI) tools were used in the preparation of this manuscript, except for the use of DeepL Pro exclusively for language translation purposes.

References

1. Pinto Santos AR, Cortés Peña OF. ¿Qué piensan los estudiantes universitarios frente a la formación investigativa? *REDU. Revista de Docencia Universitaria*. 2017;15(2):57-75. https://doi.org/10.4995/redu.2017.6059
2. Chernoff H. The Use of Faces to Represent Points in k-Dimensional Space Graphically. *J Am Stat Assoc*. 1973;68(342):361-368. https://doi.org/10.1080/01621459.1973.10482434
3. Flury B, Riedwyl H. Graphical Representation of Multivariate Data by Means of Asymmetrical Faces. *J Am Stat Assoc*. 1981;76(376):757-765. https://doi.org/10.1080/01621459.1981.10477718
4. Hananel A, Loaiza S, Collantes L. Enhancing academic performance of engineering students: A multivariate statistical analysis of grades in a Mathematics course. *Interact. Des. Archit.(s)*. 2024;63:268-299. https://doi.org/10.55612/s-5002-063-012
5. Olmos EG. Students performance: A methodology for its measurement. *Economía*. 1997;22(13):7-25. Accessed Jun 18, 2026. https://EconPapers.repec.org/RePEc:ula:econom:v:22:y:1997:i:13:p:7-25.
6. Haaf W, Friedrich K, Mayr G, Schlaich J. Solar chimneys part I: principle and construction of the pilot plant in Manzanares. *Int J Sol Energy*. 1983;2(1):3-20. http://doi.org/10.1080/01425918308909911
7. Herrada H, Jiménez M. In situ measurement of heat transfer coefficient and solar aperture of insulated dwellings using the dynamic integrated method. *Appl Therm Eng*. 2022;200. https://doi.org/10.1016/j.applthermaleng.2021.117644
8. Avial M, Chourio E, Casadei Carniel L, Vargas Z. El software matemático como herramienta para el desarrollo de habilidades del pensamiento y el mejoramiento del aprendizaje de las matemáticas. *Rev Electrón Actual Investig Educ*. 2007;7. Accessed Jun 18, 2026. https://www.redalyc.org/pdf/447/44770209.pdf.
9. Medina Martínez NF. Las variables complejas en investigaciones pedagógicas. *Apuntes Universitarios*. 2015;5(2):9-18. https://doi.org/10.17162/au.v0i2.244
10. Xu Y, Zhou X. Performance of divergent-chimney solar power plants. *Sol Energy*. 2018;170:379-387. https://doi.org/10.1016/j.solener.2018.05.068
11. Hu S, Leung DYC, Chan JCY. Numerical modelling and comparison of the performance of diffuser-type solar chimneys for power generation. *Appl Energy*. 2017;204:948-957. https://doi.org/10.1016/j.apenergy.2017.03.040
12. Mebarki A, Sekhri A, Assassi A, Hanafi A, Marir B. CFD analysis of solar chimney power plant: Finding a relationship between model minimization and its performance for use in urban areas.

Energy Rep. 2022;8:500-513. https://doi.org/10.1016/j.egyr.2021.12.008

13. Murena F, Gaggiano I, Mele B. Fluid dynamic performances of a solar chimney plant: Analysis of experimental data and CFD modelling. *Energy*. 2022;249. https://doi.org/10.1016/j.energy.2022.123
14. Cuce E, Cuce PM, Carlucci S, et al. Solar Chimney Power Plants: A Review of the Concepts, Designs and Performances. *Sustainability*. 2022;14(3):1450. https://doi.org/10.3390/su14031450
15. Biswas N, Mandal DK, Bose S, Manna NK, Benim AC. Experimental Treatment of Solar Chimney Power Plant—A Comprehensive Review. *Energies*. 2023;16(17):6134. https://doi.org/10.3390/en16176134
16. Mehranfar S, Gharehghani A, Azizi A, Mahmoudzadeh Andwari A, Pesyridis A, Jouhara H. Comparative assessment of innovative methods to improve solar chimney power plant efficiency. *Sustain Energy Technol Assess*. 2022;49:101807. https://doi.org/10.1016/j.seta.2021.101807
17. Zhu L, Khdair AI, Aghaei A, Zalipour K, Chen H, Afrand M. A comprehensive review of solar chimney power plants: technology, performance, and future prospects. *Sustain Energy Technol Assess*. 2025;81:104413. https://doi.org/10.1016/j.seta.2025.104413
18. Xiong H, Ming T, Shi T, et al. Numerical investigation on performance of solar chimney power plant with three wind resistant structures. *Energy*. 2024;297:131262. https://doi.org/10.1016/j.energy.2024.131262
19. Rahimi-Larki M, Arefian A, Nazari S, Torkfar A, Hosseini-Abardeh R, Sarlak H. Performance investigation of a sloped collector solar chimney system exposed to the ambient crosswind. *Energy*. 2025;318:134732. https://doi.org/10.1016/j.energy.2025.134732
20. Maia CB, Castro Silva JdO. CFD Analysis of a Small-Scale Solar Chimney Exposed to Ambient Crosswind. *Sustainability*. 2022;14(22):15208. https://doi.org/10.3390/su142215208
21. Arefian A, Hosseini-Abardeh R, Rahimi-Larki M, Torkfar A, Sarlak H. A comprehensive analysis of time-dependent performance of a solar chimney power plant equipped with a thermal energy storage system. *Renew Sustain Energy Rev*. 2024;189:114051. https://doi.org/10.1016/j.rser.2023.114051
22. Huang S, Li W, Lu J, Li Y, Wang Z, Zhu S. Experimental study on thermal performances of a solar chimney with and without PCM under different system inclination angles. *Energy*. 2024;290:130154. https://doi.org/10.1016/j.energy.2023.130154
23. Esmail MFC, A-Elmagid WM, Mekhail T, Al-Helal IM, Shady M. A numerical comparative study of axial flow turbines for solar chimney power plant. *Case Stud Therm Eng*. 2021;26:101046. https://doi.org/10.1016/j.csite.2021.101046
24. Caicedo P, Wood D, Johansen C. Radial Turbine Design for Solar Chimney Power Plants. *Energies*. 2021;14(3):674. https://doi.org/10.3390/en14030674
25. Fertahi SE, Moeneclaey-Masson C, Guimerà R, Belarbi R, Revol E. CFD Validation in Solar Chimney Power Plants: A Comparison of Modeling Approaches. *Fluids*. 2024;9(11):251. https://doi.org/10.3390/fluids9110251
26. Cuce PM, Cuce E, Mandal DK, et al. ANN and CFD driven research on main performance characteristics of solar chimney power plants: Impact of chimney and collector angle. *Case Stud Therm Eng*. 2024;60:104568. https://doi.org/10.1016/j.csite.2024.104568
27. Mandal DK, Gupta KK, Biswas N, Manna NK, Santra S, Benim AC. Optimization of hybrid solar chimney power plants (HSCPPs): A review of multi-objective approaches. *Appl Energy*. 2025;396:126214. https://doi.org/10.1016/j.apenergy.2025.126214
28. Nie J, Guo TZ, Xu JC, Ruan XY, Nie LYM, Guo X. CFD-based multi-location analysis of power output and LCOE for solar chimneys in arid regions of Inner Mongolia. *Case Stud Therm Eng*. 2026;79:107726. https://doi.org/10.1016/j.csite.2026.107726
29. Salameh T, Zayed M, Juaidi A, Abdallah R, Hamid AK, Hussein M. CFD and techno-economic analysis of site-dependent renewable trigeneration in solar chimney power plant. *Int J Hydrogen Energy*. 2026;205:153285. https://doi.org/10.1016/j.ijhydene.2025.153285
30. Velazco Lorenzo D, Butler Blacker JG. Desarrollo de un modelo experimental de una chimenea solar-eólica para suministro eléctrico. *TECNIA*. 2022;32(1):13-27. https://doi.org/10.21754/tecnia.v32i1.1092
31. Hananel A, Garcia R, Vera A. Optimization of solar chimney performance through CFD modelling and parametric experimental design. *Int J Optim Control Theor Appl*. 2026;16(2):428-449. https://doi.org/10.36922/IJOCTA025430181
32. Analysis of the driving potential of a solar chimney power plant. *R&D J*. 1999;15:85-94. Accessed Jun 18, 2026. http://www.scielo.org.za/scielo.php?script=sci_arttext&pid=S2309-89881999000100005&lng=en&nrm=iso.
33. Ming T, Liu W, Xu G. Analytical and numerical investigation of the solar chimney power plant systems. *Int J Energy Res*. 2006;30(11):861-873. https://doi.org/10.1002/er.1191
34. POWER NASA Project. The Prediction of Worldwide Energy Resource (POWER). NASA Applied Sciences Program within the Earth Science Division of the Science Mission Directorate; 2024. Accessed Jun 18, 2026. https://power.larc.nasa.gov/.

35. Danook SH, Al-bonsrulah HAZ, Hashim I, Veeman D. CFD Simulation of a 3D Solar Chimney Integrated with an Axial Turbine for Power Generation. *Energies*. 2021;14(18):5771. https://doi.org/10.3390/en14185771
36. Sundararaj M, Rajamurugu N, Anbarasi J, Yaknesh S, Sathyamurthy R. Parametric optimization of novel solar chimney power plant using response surface methodology. *Results Eng.* 2022;16:100633. https://doi.org/10.1016/j.rineng.2022.100633
37. Chrobak R, Sempere PG, Prieto AB, Avalos KR. Exploración sobre las estrategias de enseñanza de docentes de ingeniería para el logro de habilidades creativas e innovadoras en sus estudiantes.In: *II Congreso Internacional de Investigación y Docencia de la Creatividad*; online; 2017. https://doi.org/10.13140/RG.2.1.3061.9288
38. Cuce E, Sen H, Cuce PM. Numerical performance modelling of solar chimney power plants: Influence of chimney height for a pilot plant in Manzanares, Spain. *Sustain Energy Technol Assess.* 2020;39:100704. https://doi.org/10.1016/j.seta.2020.100704
39. Abo-Zahhad EM, Hachicha AA, Mistarihi MZ, Salim MH, Esmail MFC. Optimization of ground material properties for enhanced solar chimney power plant efficiency: A CFD and RSM approach. *Energy Rep.* 2025;13:3929-3945. https://doi.org/10.1016/j.egyr.2025.03.035
40. Torkfar A, Arefian A, Hosseini-Abardeh R, Bahrami M. Implementation of active and passive control strategies for power generation in a solar chimney power plant: A technical evaluation of Manzanares prototype. *Renew Energy.* 2023;216:118912. https://doi.org/10.1016/j.renene.2023.118912

Alberto Hananel *is a Peruvian mathematician (PhD, International Doctorate, University of Granada; Fundación Carolina scholar) and full-time faculty member at Universidad Católica Santo Toribio de Mogrovejo (USAT), Peru. He also holds a Second Specialization Degree in Engineering in Applied Statistics for Research. His research integrates finite element methods, numerical analysis of differential equations, multivariate statistics, computational fluid dynamics (CFD), and AI-assisted modeling. He has led multiple funded projects as principal investigator, including the award-winning program "Optimization of Solar Chimney Design through CFD Simulations and Multivariate Analysis with Chernoff Faces". His work appears in Scopus and Web of Science indexed journals, as well as books and conference proceedings, with a focus on computational and optimization approaches for engineering applications, particularly in renewable energy and data-driven decision-making.*
https://orcid.org/0000-0003-4113-8623

Rodolfo García *is a Professor at the Faculty of Engineering and Architecture of Universidad Católica Santo Toribio de Mogrovejo (USAT), Peru, where he conducts research in Computational Fluid Dynamics (CFD) and its applications to renewable energy and thermal systems. He holds a Master's degree in Advanced Mechanical Engineering from the University of Warwick, supported by the "Beca Generación del Bicentenario" scholarship. His work focuses on CFD modeling, heat transfer optimization, and fluid–structure interaction. He has participated in multidisciplinary projects involving solar energy systems and industrial process optimization. His research aims to bridge theory and practice through computational techniques that improve engineering performance and energy efficiency, and he develops numerical strategies for fluid-driven energy systems, collaborating with national and international institutions.*
https://orcid.org/0000-0002-9541-6257

Alejandro Vera *holds a PhD in Science and Engineering, specializing in Mechanical Vibrations using wavelet and Hilbert–Huang Transform (HHT) analysis. He also holds a Master's degree in Mechanical and Electrical Engineering (Energy major, UNPRG–CARELEC) and a Bachelor's degree in Mechanical Engineering (UNT, Peru). He specializes in energy efficiency, industrial energy planning, ISO 50001 implementation, and vibration analysis of rotating machinery. He works as an independent consultant in reliability engineering, applying predictive techniques with Matlab and Power BI, and has contributed to the digitalization and energy transition of hydroelectric power plants. His professional work integrates advanced diagnostic techniques for condition monitoring and predictive maintenance in energy systems. At USAT, Peru, he conducts research and teaches in mechanical design, reliability engineering, energy systems, and asset management.*
https://orcid.org/0000-0003-0198-338X

Sandra Cecilia Loaiza Chumacero *is a Lecturer at the Faculty of Engineering of Universidad Católica Santo Toribio de Mogrovejo (USAT), Peru, where she teaches undergraduate and graduate courses in Descriptive and Inferential Statistics. She holds a Bachelor's degree in Statistics and a Master's degree in Education Sciences with a specialization in Cognitive Psychopedagogy from Universidad Nacional Pedro Ruiz Gallo, Peru. Her experience includes statistics education, applied statistics for engineering, health sciences, psychology, and social sciences, as well as research methodology and thesis supervision. Her research interests include statistical modeling in education and social sciences, applied regression methods, information literacy, and educational data analysis. She has authored scientific articles, book chapters, and conference papers published in indexed journals and international proceedings, and collaborates in interdisciplinary research on educational innovation and applied statistical analysis.*
https://orcid.org/0000-0002-0311-1692

Iván Dennys Soto Rodríguez *is a Statistical Engineer from Universidad Nacional Agraria La Molina (UNALM), Peru, where he serves as a Full Professor in Statistics and Informatics at undergraduate and graduate levels. He holds a Master's degree in Computer Science from Pontificia Universidad Católica del Perú (PUCP) and a PhD in Development and Strategic Security from CAEN, Peru. His career spans more than three decades, combining teaching, public-sector leadership, and applied research. He has held senior positions at the National Institute of Agrarian Innovation (INIA), contributing to experimental statistics, project evaluation, and agricultural data analysis, including work with geographic information systems and multivariate techniques. His research interests include experimental design, multivariate statistics, data science, educational statistics, and information systems, with publications in indexed journals, conference proceedings, and academic books.*
https://orcid.org/0000-0002-4928-8362

An International Journal of Optimization and Control: Theories & Applications (https://accscience.com/journal/ijocta)



This work is licensed under a Creative Commons Attribution 4.0 International License. The authors retain ownership of the copyright for their article, but they allow anyone to download, reuse, reprint, modify, distribute, and/or copy articles in IJOCTA, so long as the original authors and source are credited. To see the complete license contents, please visit http://creativecommons.org/licenses/by/4.0/.